Hybrid Solar Thermal/PV Receiver with Thin Film Solar Cell as Secondary Concentrator

Lun Jiang[1,2], *Bennett Widyolar[1,2], Jon Ferry[1,2], Jordyn Brinkley[1,2], Roland Winston[1,2], David Cygan[3], Hamid Abbasi[3]

[1] University of California, Merced (USA)

[2] Advanced Solar Research Institute (UC Solar), Merced (USA)

[3]Gas Technology Institute, Chicago (USA)

Abstract

A hybrid concentrating photovoltaic / concentrating solar power spectrum splitting collector has been designed, developed, and experimentally tested in a joint effort by the Gas Technology Institute (GTI) and the University of California, Merced (UCM), sponsored by the U.S. Department of Energy (DOE) Advanced Research Project Agency - Energy (ARPA-E). The two-stage optical system pairs a parabolic trough with a compound parabolic concentrating (CPC) secondary concentrator, generating 50X geometric concentration on the thermal absorber. Dual-junction indium gallium phosphide/gallium arsenide (InGaP/GaAs) solar cells integrated into the secondary reflector generate electricity from photons with energy greater than ~1.4 eV and reflect the remaining lower energy infrared photons to the thermal absorber for optimal spectral utilization. The collector has been developed into a working prototype and tested on-sun up to 600 °C (hybrid collector) and 685 °C (thermal-only collector). The prototype collector demonstrated 63% optical efficiency and 40% thermal efficiency at 650 °C. This work demonstrates a two-stage linear parabolic trough collector, back-reflecting solar cells which operate as spectrum splitting devices, and a solid particulate heat transfer fluid which enables high temperature operation beyond existing heat transfer fluids. As a result, the team is now developing a more robust optical design which is collapsed to allow drop-in retrofit with commercial parabolic trough collectors.

Keywords: Solar, Hybrid, Spectral Beam Splitting, CSP, CPV, InGaP, GaAs

1. Introduction

Hybrid solar photovoltaic/thermal (PV/T) collectors produce both heat and electricity in a single system. Most current PV-T systems operate by using a heat transfer fluid (HTF) to capture and use the excess heat generated by the solar cell. While most of the incident solar energy can be harvested, these systems are limited by the temperature and conversion efficiency of the solar cells which limits them to low temperature operation (<100 °C) where the thermal component in less useful for power generating applications. Selectively controlling the solar spectrum through spectral beam splitting (SBS) enables hybrid PV/T collectors where the PV and thermal components are *thermally decoupled.* This allows the thermal component to operate at high temperatures where it becomes valuable for power generation without hindering the performance of the solar cell component. By reaching higher conversion efficiencies, these collectors can reduce electricity costs from hybrid CSP/CPV power generating plants compared to traditional CSP and by doing so provide an intermediate solution to incentivize deployment of dispatchable thermal energy storage (TES) (Branz et al. 2015).

The team at Gas Technology Institute (GTI) and the University of California, Merced (UCM) have developed a novel hybrid PV/T solar collector. The proposed collector incorporates dual-junction InGaP/GaAs back-reflecting solar cells in a secondary reflector. In this way they function as a CPV subsystem, generating electric current from high energy photons, but also as beam splitting devices by reflecting low energy photons to the CSP subsystem (absorber) at the focus of the secondary concentrator. The design and development of this technology is discussed in this manuscript.

2. Collector Design

doi:10.18086/swc.2019.05.06 Available at http://proceedings.ises.org

The geometric concentration ratio of typical parabolic trough systems concentrating onto cylindrical absorbers is given by Equation (1), where φ is the half-rim-angle of the parabola and θ is the half-acceptance-angle.

$$C_{PTC} = \frac{\sin\phi}{\pi \sin\theta} \qquad \text{(Eq. 1)}$$

Parabolic systems are typically designed with φ close to 90° to maximize their concentration and when this is the case the concentration ratio reduces to $(\pi.\sin\theta)^{-1}$ or roughly 30X for a half-acceptance angle $\theta = 0.6°$. The thermodynamic limit for concentration in a 2D system with a faraway source is given by Equation (2) (Winston 1970).

$$C_{max} = \frac{1}{\sin\theta} \qquad \text{(Eq. 2)}$$

Therefore, it should be possible to increase the geometric concentration ratio of typical trough systems by a factor of π. One approach is to use a secondary concentrator for which the total concentration ratio of the two-stage system using an ideal secondary concentrator can be calculated from Equation (3) (Collares-Pereira et al. 1991).

$$C_{two-stage\ PTC} = \frac{\cos\phi}{\theta} \qquad \text{(Eq. 3)}$$

The concentration maximizes for small half rim angles, but long focal lengths make anything smaller than 45° impractical. The secondary aperture area (A_2) is defined by Equation (4).

$$A_2 = \frac{A_1\theta}{\sin\phi\cos\phi} \qquad \text{(Eq. 4)}$$

Where, A_1 is the primary concentrator aperture width. For this design, the primary concentrator is a 5 m wide 45° half-rim angle parabolic reflector which reflects and focuses light into a 45° half-angle beam on the secondary concentrator at a focal distance (f) of 3.02 m. The secondary concentrator is a compound parabolic concentrator (CPC) which accepts light within a 45° half-angle spread reflected by the primary mirror and further concentrates it onto the thermal absorber area (A_3). A half-acceptance angle $\theta = 0.6°$ yields a secondary aperture width of 105 mm. This allows the entire PV/T receiver (secondary reflector and thermal absorber) to fit inside a standard 120 mm glass cover tube and accommodates the 0.25° sun disk half angle and other optical inaccuracies in the system such as mirror imperfections, structural bending, and optical misalignment. The maximum theoretical geometric concentration ratio approaches 68X (Schmitz et al. 2015).

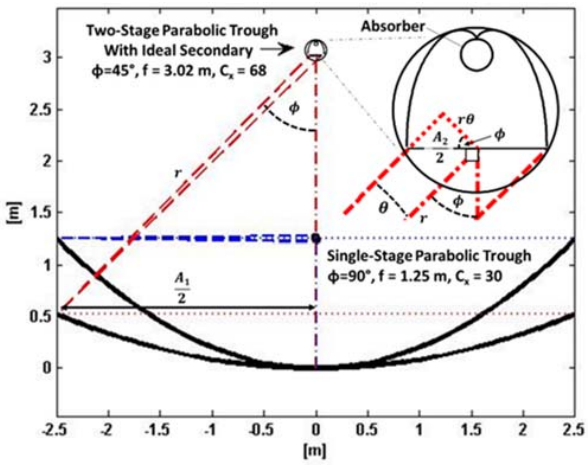

Fig. 1: Two stage parabolic trough collector (PTC) design (red) overlaying typical single-stage PTC design (blue).

Sections of the CPC are replaced with high efficiency back-reflecting solar cells which directly generate electricity using above-bandgap photons while reflecting sub-bandgap photons to the thermal absorber. To optimize placement of the solar cells, ray trace simulations were performed and the resulting intensity profile along the CPC reflector was used to determine the ideal location for the solar cells (10 mm from the center of the CPC profile and extending approximately 50 mm). Since the solar cells cannot be bent, the CPC profile was approximated by flat segments. Ray trace simulations for a CPC using 4 strips of 16 mm wide flat segments showed geometric efficiencies at 90% of the ideal. To recover this loss, a new design (Widyolar et al. 2017b) that

guarantees edge ray incidence on the absorber was developed (Figure 2) and by doing so the geometric efficiency was fully recovered at the expense of a 13% reduction in aperture area (concentration ratio). To maintain the required aperture, the entire secondary design was scaled up to a final secondary aperture width of 110 mm and an absorber outer diameter (OD) of 32 mm. After these changes, the system has a final geometric concentration ratio of $Cx = \frac{5000\ mm}{\pi * 32\ mm} = 50$. The final parameters of the two-stage optical system are listed in Table 1.

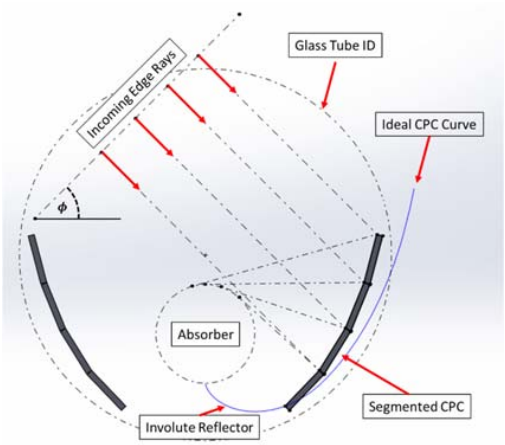

Fig. 2: Optimized secondary CPC shape where portions of profile are approximated by flat segments. Optimized profile has 100% geometric efficiency despite non-ideal shape [27].

Table 1: Two-Stages Concentrator Parameters

Design Parameter	Value
ϕ	45°
θ	0.6°
A_1	5 m
A_2	110 mm
A_3	100 mm
C_1	45X
C_2	1.1X
C_{total}	50X

Dual-junction Gallium Arsenide (GaAs) / InGaP were selected for use as beam splitting solar cells. To demonstrate the beam splitting capability of these cells, the external quantum efficiency (EQE), open circuit voltage (V_{oc}), and fill factor (FF) were taken from the solar cell efficiency tables and used to calculate spectral efficiency $\eta_{cell}(\lambda)$ using Equation (5), where q is the elementary charge in coulombs, h is the Planck constant, c is the speed of light, and λ is the wavelength of light.

$$\eta_{cell}(\lambda) = q\frac{\lambda}{hc}EQE(\lambda)\,V_{oc}\,FF \qquad \text{(Eq. 5)}$$

The spectral efficiency of InGaP (dashed blue) and GaAs (dashed red) are plotted against the direct-beam solar spectrum in Figure 3. The in-band efficiency (η_{band}) calculated according to Equation (6) is the solar cell's effective efficiency within the spectral window bound by λ_1 and λ_2. These are also shown in for each cell above the x-axis in Figure 3.

$$\eta_{band} = \frac{\int_{\lambda_1}^{\lambda_2}\eta_{cell}(\lambda)G_{direct}(\lambda)}{\int_{\lambda_1}^{\lambda_2}G_{direct}(\lambda)} \qquad \text{(Eq. 6)}$$

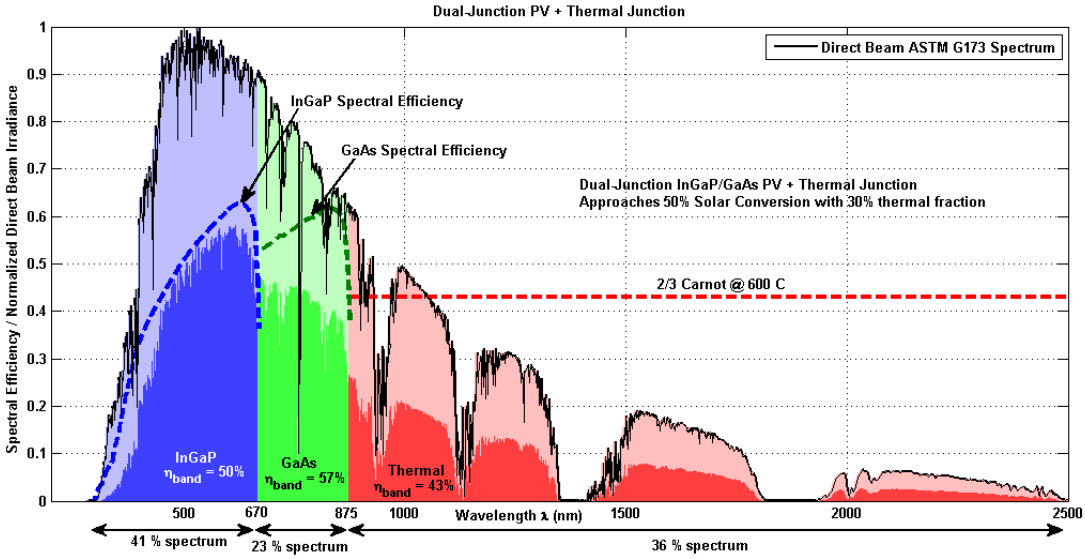

Fig. 3: Spectral beam splitting with dual-junction PV and third thermal junction. InGaP and GaAs spectral efficiency curves (dashed blue and green) are adapted from the solar cell efficiency tables.

The Carnot efficiency (η_{Carnot}) is calculated using Equation (7), where T_H is the hot reservoir temperature and T_c is the cold reservoir temperature.

$$\eta_{Carnot} = 1 - \frac{T_C}{T_H} \qquad \text{(Eq. 7)}$$

Engines typically only reach 2/3 of this limit and this efficiency is plotted (dashed red) for a target operating temperature (T_H) of 600 °C and cold reservoir temperature (T_C) of 37 °C and is listed as η_{band} for the thermal junction in Figure 3. Also listed below the x-axis are the fractions of the direct beam solar spectrum within each spectral region from 0-670 nm, 670-875 nm, and 875-2500 nm.

The in-band efficiency of each junction multiplied by the fraction of the solar spectrum in each band yields a total solar-to-electric conversion efficiency of 49.1%. This is higher than what is achieved by any of the subsystems under full spectrum alone. While optical, thermal, and conversion losses will reduce this number in practice, this demonstrates the potential of beam splitting systems to achieve higher conversion efficiencies through optimal utilization of the solar spectrum.

3. Prototype Development & Testing

Receiver Prototype

Two receiver configurations were developed into prototypes: a hybrid version with dual-junction InGaP/GaAs cells incorporated into the secondary reflector, and a thermal-only version with just the secondary reflector. A collapsed and exploded view of the hybrid receiver is shown in Figure 4.

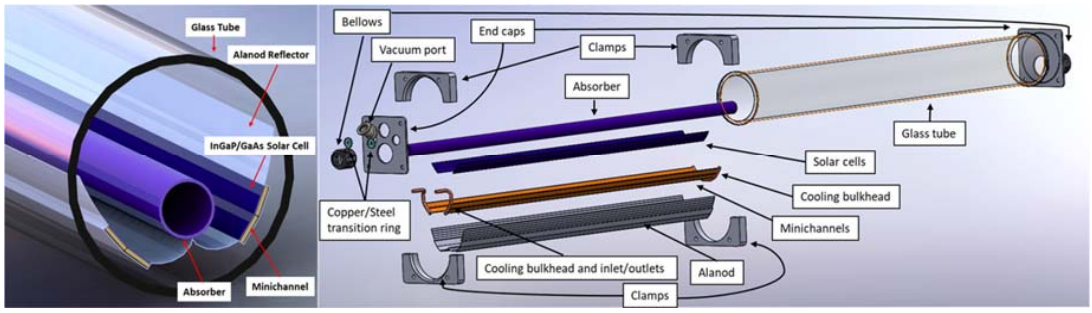

Fig. 4: Hybrid receiver design (left) and exploded view of components (right)

The actual finished prototypes are pictured in Figure 5. On the far right you can see the full aperture of the secondary appears to be dark green, indicating proper operation of the secondary optics which are directing rays from the absorber to the camera.

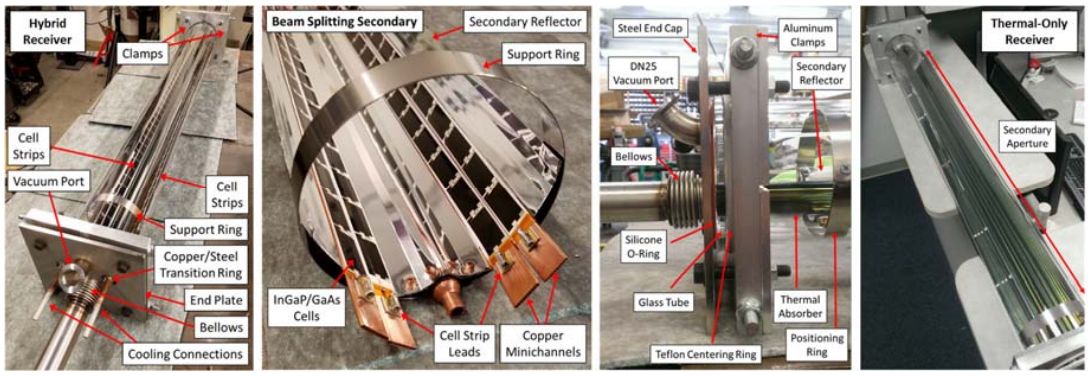

Fig. 5: Assembled hybrid receiver (left), beam splitting hybrid secondary (middle left), thermal-only end cap (middle right), assembled thermal-only receiver (right).

Experimental tests were carried out at the University of California, Merced Castle Research Facility (37.3 °N, 120.6 °W) jointly with GTI. Optical efficiency tests were performed first using city water as the HTF, after which high temperatures tests were carried out using a solid particulate HTF transport and storage rig developed by GTI.

A combination of high-temperature ceramic heaters located on the rig and on the supply pipeline on the tracker (labeled as auxiliary heaters) were used to add heat into the HTF to allow extensive testing during non-ideal on-sun conditions. The entire piping system was insulated with 1" of aerogel insulation and external layers of FiberFrax insulation. In-flow thermocouple clusters installed at the inlet and outlet of the receiver thermal stream measured the temperature rise across the collector. The mass flow rate of particles was calculated by the change in the feed hopper load cell output over time. The heat capacity of the particulate HTF was assumed to be a constant 0.8 kJ/kg-K. The thermal efficiency of the thermal stream was calculated from equation 10.

$$\eta_{thermal} = \frac{Q_{thermal}}{Q_{solar}} = \frac{\dot{m} c_p \Delta T}{A_1 DNI} \qquad (10)$$

The cooling circuit was fed by a city-water line. The flow rate of water through the minichannels was measured manually by recording the time it took to fill a 5-gallon bucket (which actually contains 5.6 gallons). Flow rates were typically around 25 g/s to facilitate ~ 10 ΔT in the cooling circuit for thermocouple error reduction. Inlet and outlet temperatures of the cooling circuit were measured manually using a hand-held thermocouple reader by inserting a thermocouple probe directly into the flow. The heat capacity of water was assumed to be a constant 4.184 kJ/kg-K and the cooling circuit efficiency (the fraction of incoming solar exhausted as waste heat) was calculated according to equation 10.

The performance of each strip of solar cells was quantified using a Keithley 2460 *I-V* curve tracer. The maximum power output ($I_m V_m$) of each strip of cells was determined and added to estimate net solar-to-electric efficiency of the CPV subsystem according to equation 11.

$$\eta_{electric} = \frac{\Sigma_{strips}^{4} I_m V_m}{A_1 DNI} \qquad (11)$$

The vacuum in the receiver was actively maintained by a benchtop combination (turbopump + roughing pump) vacuum station. It was connected to the bottom of the receiver by 3 meters of flexible hose and a vacuum gauge at the opposite end of the receiver was used to measure vacuum pressure inside the receiver.

The hybrid collector was tested during May, November, and December of 2017 (Figure 6). Initial optical efficiency tests were performed using water as the HTF since its properties are well known. There was no vacuum during this test, but this should have little effect since the collector was operating near ambient conditions. *I-V* curve tracing was performed on all four strips of cells, resulting in a maximum solar-to-electric efficiency of the

cell subsystem of 4%.

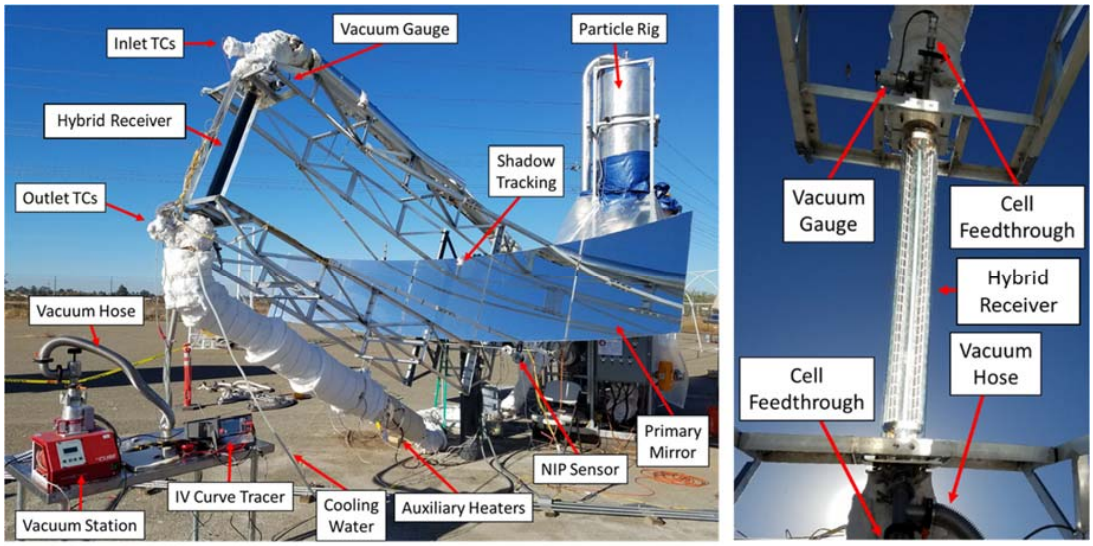

Fig. 6: Experimental setup with hybrid receiver (left), hybrid receiver on-sun (right)

Table 2: Hybrid collector test results

Date	Duration	Thermal Stream HTF	Thermal Stream Temp	Average Thermal Efficiency	Cooling Temp	Cell Thermal Generation*	Cell Electric Efficiency	Receiver Internal Pressure
5/17/2017	3 hrs	Water	40 °C	64%	20-35 °C	17%	4%	Atmospheric
11/18/2017	11 hrs	Particles	600 °C	15%	20-29 °C	19%	3.6%	1.9 e^{-3} mbar
12/4/2017	1 hr	Particles	50 °C	63%	16-26 °C	16%	-	1.2 e^{-2} mbar
12/5/2017	3 hrs	Particles	100 °C	62%	23-28 °C	12%	-	1.4 e^{-2} mbar

After optical testing, the collector was connected to the particle transport rig for high temperature testing. Starting at midnight on November 18th, 2017 the system was warmed up until the receiver outlet reached a stable 600 °C by 10 am. The temperature profiles during the test are shown in Figure 7. The receiver was evacuated, reaching a lowest internal pressure of 1.9×10^{-3} mbar. *I-V* curve tracing was performed on all four strips of cells (Figure 7), however, only three strips were active as one strip became disconnected during a vacuum-seal repair). The maximum power for all three strips was about 42 Watts (60 V and 0.7 A) and this was assumed for the fourth strip in the estimation of cell electric efficiency.

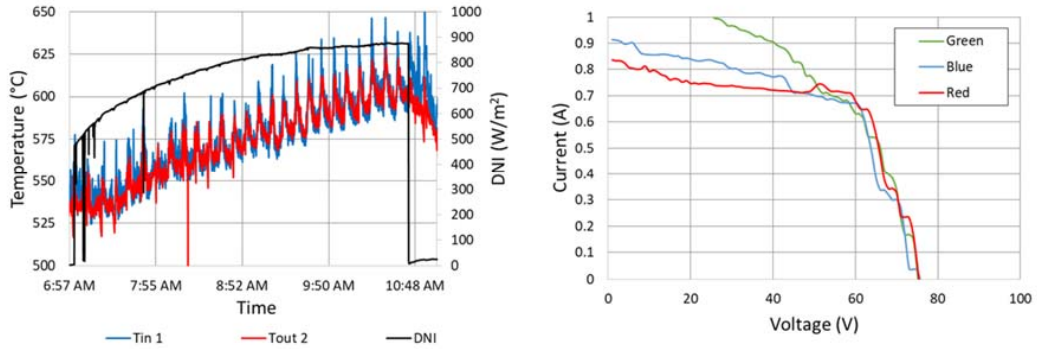

Fig. 7: Hybrid receiver temperatures during 600 °C test (left), hybrid receiver IV-curves during 600 °C test (right).

On December 4th, 2017 a second optical efficiency test was performed, this time using particles). The thermal efficiency with particles was nearly identical to the earlier optical efficiency tests with water, indicating little to no degradation of the hybrid receiver operated under slowly increasing temperatures up to 250 °C peak. Cell performance was not quantified in these last two tests.

The thermal-only collector was tested between August – November 2017 (Figure 8) in the same way as the hybrid collector, but without the solar cell cooling or IV curve tracing.

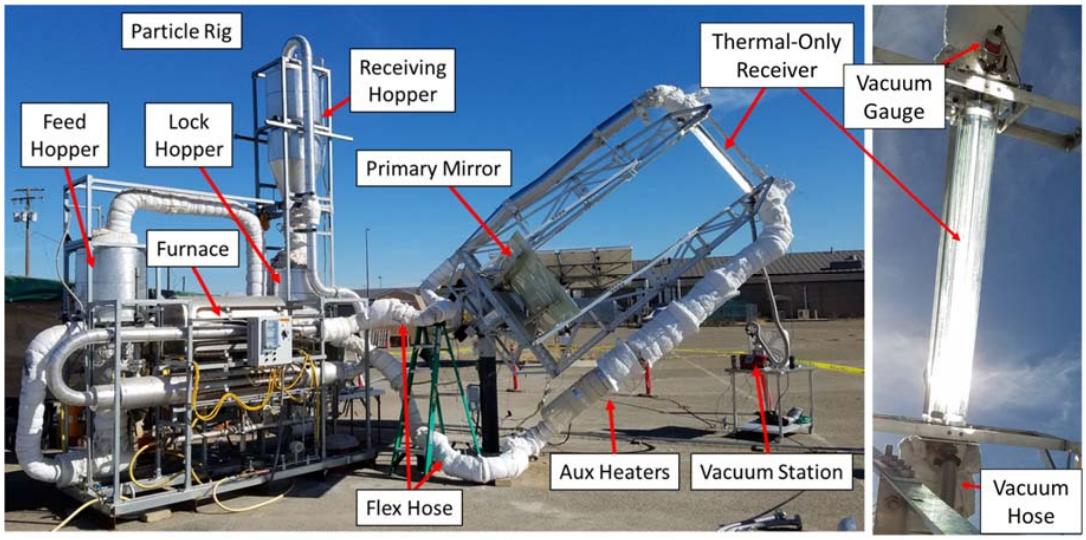

Fig. 8: Experimental setup with thermal-only receiver (left), thermal-only receiver on-sun (right).

The results from experimental testing are summarized in Fig. 9 with a second order polynomial curve fit. The first point on the top left is the result of multiple tests using water. The remaining points are taken using a particulate HTF.

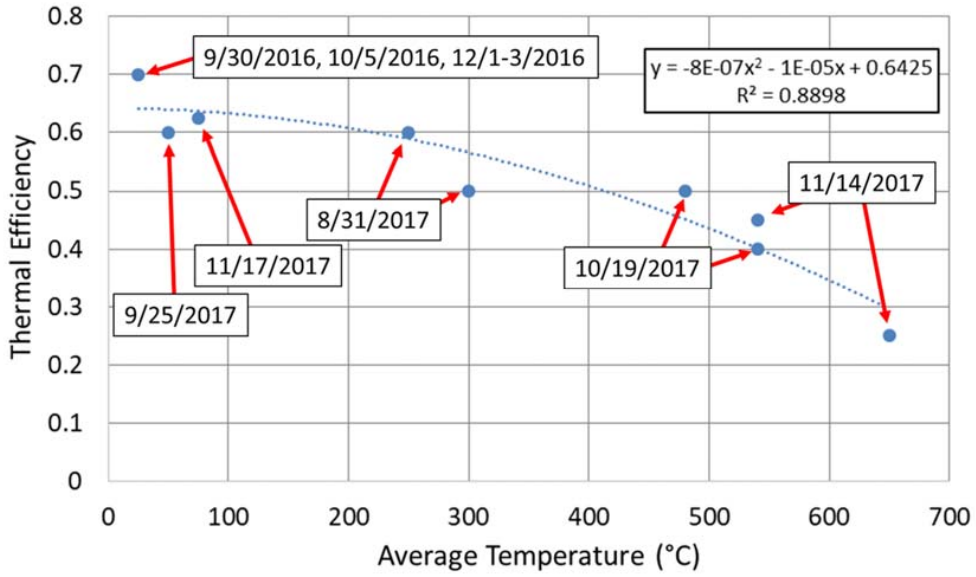

Fig. 9: Experimental results of thermal-only collector testing.

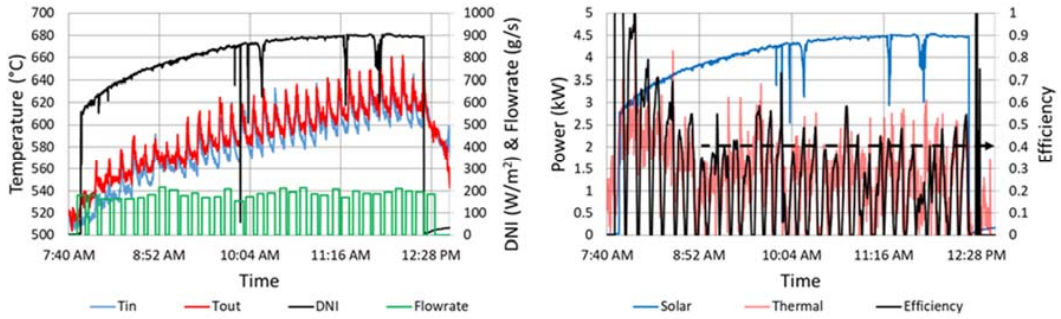

Fig. 10: Experimental results of thermal-only during 650 °C test showing the solar resource, thermal temperatures, and flow rate (left) and the calculated solar power, thermal power, and efficiency (right).

By the end of testing the thermal receiver had undergone over 50 hours of operation and was dismounted with no visual indication of any degradation (Figure 11). Based on these experimental results the collector achieved a thermal efficiency of 40% at a particle temperature of 650 °C.

Fig. 11: Thermal receiver after 50 hours of continuous operation.

4. Conclusions and Future Work

A hybrid solar collector using a two-stage parabolic trough with a compound parabolic optical system and dual-junction InGaP/GaAs solar cells was developed and demonstrated by the GTI / UCM team. The hybrid and thermal-only receivers were operated up to 600 °C and 685 °C, respectively, without failure. The two-stage linear trough system, which pairs a secondary compound parabolic reflector with a primary parabolic trough, enables much higher concentration ratios than existing technologies (50X compared to 23X) and higher temperature operation, even under partial illumination (spectrum splitting). Back-reflecting solar cells provide spectrum splitting and can be a tool for high exergy solar-to-electric generation as they eliminate the need for additional optical or light-filtering materials. Furthermore, the use of an internally flowing solid particulate heat transfer fluid was demonstrated for the first time in an actual prototype collector system with several meters of pipe and flex hose. Solid particles allow an increase in operating temperature beyond the 400 °C limit of thermal oils and the 580 °C limit of current molten salts. High temperatures are particularly beneficial for thermal storage and improving the thermal-to-electric conversion efficiencies of turbines. In particular, the pairing of the two-stage trough and solid particulate heat transfer fluid enables high temperature operation from a linear solar system within the realm of tower technologies which presents an exciting new opportunity for industrial process heating and concentrating solar power applications. As a result, the team is now developing a full scale *collapsed* collector design which will allow drop-in retrofit with existing parabolic trough collectors. Initial techno-economic analysis has revealed a levelized cost of heat (LCOH) of approximately $0.03/kWh delivered at 650 °C over 25 years, which is comparable the price of natural gas in California.

5. Acknowledgement

This work was performed with financial support from the Advanced Research Projects Agency-Energy (ARPA-E) under grant ARPA-E DE-AR0000464 awarded to the Gas Technology Institute by the US Department of

Energy (DOE). The authors wish to thank our partner Microlink Devices (Alex Kirk, Drew Brees, Mark Osowski) for developing and supplying the high efficiency dual-junction thin film solar cells applied to the minichannels.

6. References

Abdelhamid, M., Widyolar, B.K., Jiang, L., Winston, R., Yablonovitch, E., Scranton, G., Cygan, D., Abbasi, H. and Kozlov, A., 2016. Novel double-stage high-concentrated solar hybrid photovoltaic/thermal (PV/T) collector with nonimaging optics and GaAs solar cells reflector. Applied Energy, 182, pp.68-79.

Branz, H.M., Regan, W., Gerst, K.J., Borak, J.B. and Santori, E.A., 2015. Hybrid solar converters for maximum exergy and inexpensive dispatchable electricity. Energy & Environmental Science, 8, pp.3083-3091.

Brinkley, J. and Hassanzadeh, A., 2017. Adaptive sensor-based ultra-high accuracy solar concentrator tracker. In Nonimaging Optics: Efficient Design for Illumination and Solar Concentration XIV. 10379, 1037909

Collares-Pereira, M., Gordon, J.M., Rabl, A. and Winston, R., 1991. High concentration two-stage optics for parabolic trough solar collectors with tubular absorber and large rim angle. Solar Energy, 47, pp.457-466

Cygan, D., Abbasi, H., Kozlov, A., Pondo, J., Winston, R., Widyolar, B., Jiang, L., Abdelhamid, M., Kirk, A.P., Drees, M. and Miyamoto, H., 2016. Full Spectrum Solar System: Hybrid Concentrated Photovoltaic/Concentrated Solar Power (CPV-CSP). MRS Advances, 1(43), pp.2941-2946.

Dunham, M.T. and Iverson, B.D., 2014. High-efficiency thermodynamic power cycles for concentrated solar power systems. Renewable and Sustainable Energy Reviews, 30, pp.758-770.

Ju, X., Xu, C., Han, X., Du, X., Wei, G. and Yang, Y., 2017. A review of the concentrated photovoltaic/thermal (CPVT) hybrid solar systems based on the spectral beam splitting technology. Applied Energy, 187, pp.534-563.

Schmitz, M., Cooper, T., Ambrosetti, G. and Steinfeld, A., 2015. Two-stage solar concentrators based on parabolic troughs: asymmetric versus symmetric designs. Applied optics, 54, pp.9709-9721.

Selvakumar, N. and Barshilia, H.C., 2012. Review of physical vapor deposited (PVD) spectrally selective coatings for mid-and high-temperature solar thermal applications. Solar Energy Materials and Solar Cells, 98, pp.1-23

Widyolar, B.K., Abdelhamid, M., Jiang, L., Winston, R., Yablonovitch, E., Scranton, G., Cygan, D., Abbasi, H. and Kozlov, A., 2017a. Design, simulation and experimental characterization of a novel parabolic trough hybrid solar photovoltaic/thermal (PV/T) collector. Renewable Energy, 101, pp.1379-1389.

Widyolar, B., Jiang, L. and Winston, R., 2017b. Thermodynamics and the segmented compound parabolic concentrator. Journal of Photonics for Energy, 7(2), pp.028002-028002.

Widyolar, B., Jiang, L., Ferry, J., Winston, R., Kirk, A., Osowski, M., Cygan, D. and Abbasi, H., 2018, September. Two-stage 50X hybrid spectrum splitting CSP/CPV collector with InGaP/GaAs solar cells. In Nonimaging Optics: Efficient Design for Illumination and Solar Concentration XV (Vol. 10758, p. 1075806). International Society for Optics and Photonics.

Widyolar, B., Jiang, L. and Winston, R., 2018. Spectral beam splitting in hybrid PV/T parabolic trough systems for power generation. Applied Energy, 209, pp.236-250.

Widyolar, B., Jiang, L., Ferry, J., Winston, R., Kirk, A., Osowski, M., Cygan, D. and Abbasi, H., 2019. Theoretical and experimental performance of a two-stage (50X) hybrid spectrum splitting solar collector tested to 600° C. Applied energy, 239, pp.514-525.

Widyolar, B., Jiang, L., Ferry, J., Winston, R., Cygan, D. and Abbasi, H., 2019. Experimental performance of a two-stage (50×) parabolic trough collector tested to 650° C using a suspended particulate heat transfer fluid. Applied energy, 240, pp.436-445.

Winston, R., 1970. Light collection within the framework of geometrical optics. JOSA, 60, pp.245-247.

Winston, R., Yablonovitch, E., Jiang, L., Widyolar, B., Abdelhamid, M., Scranton, G., Cygan, D. and Kozlov, A., 2015, August. Hybrid solar collector using nonimaging optics and photovoltaic components. In Proc. of SPIE (Vol. 9572).

Winston, R., Jiang, L., Abdelhamid, M., Widyolar, B.K., Ferry, J., Cygan, D., Abbasi, H., Kozlov, A., Kirk, A., Elarde, V. and Osowski, M., 2016, September. Nonimaging optics maximizing exergy for hybrid solar system. In SPIE Optical Engineering+ Applications (pp. 99550N-99550N). International Society for Optics and Photonics